

Article

Study on the High Temperature Interfacial Stability of Ti/Mo/Yb_{0.3}Co₄Sb₁₂ Thermoelectric Joints

Ming Gu, Shengqiang Bai *, Xugui Xia, Xiangyang Huang, Xiaoya Li, Xun Shi and Lidong Chen

State Key Laboratory of High Performance Ceramics and Superfine Microstructure, Shanghai Institute of Ceramics, Chinese Academy of Sciences, 1295 Dingxi Road, Shanghai 200050, China; ftgm@mail.sic.ac.cn (M.G.); xgxia@mail.sic.ac.cn (X.X.); xyhuang@hotmail.com (X.H.); xyli@mail.sic.ac.cn (X.L.); xshi@mail.sic.ac.cn (X.S.); cld@mail.sic.ac.cn (L.C.)

* Correspondence: bsq@mail.sic.ac.cn; Tel.: +86-021-6916-3686

Received: 31 August 2017; Accepted: 13 September 2017; Published: 15 September 2017

Abstract: To improve the interfacial stability at high temperatures, *n*-type skutterudite (SKD) thermoelectric joints with sandwich structures of Ti/Mo/Yb_{0.3}Co₄Sb₁₂ were successfully designed and fabricated. In this structure, Mo and Ti were introduced as the barrier layer with the goal of suppressing the interfacial diffusion and the buffer layer with the goal of enhancing the bonding strength, respectively. To evaluate the high temperature interfacial behavior of the Ti/Mo/Yb_{0.3}Co₄Sb₁₂ joints, thermal shocking between 0 °C and 600 °C and isothermal aging at a temperature range of 550 °C to 650 °C were carried out in vacuum. During the isothermal aging process, Ti penetrates across the Mo layer, and finally diffuses into the Yb_{0.3}Co₄Sb₁₂ matrix. By increasing the isothermal aging time, Ti continuously diffuses and reacts with the elements of Sb and Co in the matrix, consequently forming the multilayer-structured intermetallic compounds of Ti₃Sb/Ti₂Sb/TiCoSb. Diffusion kinetics was investigated and it was found that the interfacial evolution of the Ti/Mo/Yb_{0.3}Co₄Sb₁₂ joints was a diffusion-controlling process. During the diffusion process, the formed Mo-Ti buffer layer acts as a damper, which greatly decelerates the diffusion of Ti towards the Yb_{0.3}Co₄Sb₁₂ matrix at high temperatures. Meanwhile, it was found that the increase in the contact resistivity of the joints mainly derives from the inter-diffusion between Ti and Yb_{0.3}Co₄Sb₁₂. As a result, the Ti/Mo/Yb_{0.3}Co₄Sb₁₂ joint demonstrates the excellent stability of the interfacial contact resistivity. Service life prediction was made based on the stability of the contact resistivity, and it was found that the Ti/Mo/Yb_{0.3}Co₄Sb₁₂ joint is qualified for practical applications at 550 °C.

Keywords: thermoelectric joint; skutterudite; diffusion kinetics; contact resistivity; service life prediction

1. Introduction

Unlike traditional power generation systems, a thermoelectric power generator (TEG) produces electrical power based on the Seebeck effect, via the movement of charge carriers within thermoelectric materials under a temperature difference. Using the heat from radioisotopes, TEGs can supply electrical power for tens of years, and are now the only choice of power source for deep space explorers which fly far from the sun and therefore can no longer obtain sufficient sunlight energy [1,2]. In the past decade, TEGs have been regarded as one of the most promising candidates to recover waste heat from industries or automobiles and turn them into electricity [3,4], which can benefit from the remission of the fossil energy shortage and global warming. Recently, TEGs have become one of the research focuses, and are expected to act as power suppliers of wearable electronic equipment [5].

Intrinsically, the performance of a TEG depends on the property of the thermoelectric (TE) material, which is referred to as the dimensionless figure of merit of *ZT*. Among the investigated

various systems of TE materials, silicides [6–9], half-Heuslers [10,11], and tellurides (e.g., of Bi [12–14], Pb [15–18] and Ge [19,20]) have been widely studied and some have been practically applied in TEGs. Besides, a number of materials featuring excellent TE properties (high ZT value) and a relatively lower cost, low toxicity, and good mechanical properties, such as filled skutterudite (SKD), also attract extensive attention and have been actively pursued for being converted into TEGs [21–26].

Thermoelectric joints, consisting of TE materials and electrodes, are the fundamental parts and also the key components of a TEG. In practical applications, the performance of a TEG not only depends on the property of TE materials, but also depends on the temperature difference between the hot- and cold-sides of the TE material bulks. Higher hot-side temperatures usually lead to a larger temperature difference, further enhancing the performance of the TEG. Meanwhile, a higher hot-side temperature also encourages interfacial diffusion and accelerates the degradation of the contact property, especially the contact (electrical) resistivity, which definitely deteriorates the performance and stability of the TEGs.

Practically, the high temperature TEGs are expected to perform stably for a couple of years or even longer. For example, to make full use of the TE property, the hot side temperature of the CoSb₃-based SKD joints should be 500 °C or higher. At such a high temperature, the major component in the SKD material, antimony, will react fiercely with most electrode materials (Cu, Ni, and Al, etc.) and then form single- or multi-layer interfacial intermetallics (IMC). The performance and stability of the TE joints are sensitively influenced by the microstructure and properties of the interface between the TE materials and electrode. To improve the interfacial stability of the SKD joints, a diffusion barrier layer is usually inserted between the electrode and the SKD material. Fan et al. firstly reported using Ti as the barrier layer in the CoSb₃ [27]. Zhao et al. systematically studied the diffusion kinetics of the Ti/CoSb₃ interface at high temperatures and predicted a service life of over 20 years for Ti/CoSb₃ joints at 500 °C, using interfacial shearing strength as the criteria [28,29]. In Zhao's work, when the working temperature increased to 550 °C, the diffusion speed at the Ti/CoSb₃ interface increased by one order and the predicted service life dropped to within one year [28]. In 2014, similar interfacial evolution in Ti/Yb_{0.6}Co₄Sb₁₂ joints was found and the method was developed to improve the interfacial stability of CoSb₃-based *n*-type SKD joints by introducing a Ti-Al barrier layer [30]. However, the uneven distributions of Ti and Al at the interfaces leave the accurate measurements of the thickness of the interfacial diffusion layer incomplete. Therefore, the diffusion kinetics and life prediction were also not studied. Afterwards, Fan et al. designed a Ti-Mo mixture as the barrier layer for the *n*-type Yb_{0.3}Co₄Sb₁₂ matrix and found that the dispersion of the chemically stable Mo particles (≤ 15 %) disturbs the inter-diffusion between the Ti and Yb_{0.3}Co₄Sb₁₂ matrix, which results in an improved interfacial stability at 550 °C. Still, the diffusion kinetics and life prediction were not studied [31]. Besides, Bae et al. studied the stability of the power generation characteristics of the Mo-Cu/Ti/SKD joints in terms of vibration and thermal cycling, and found that Ti helps to achieve good interfacial bonding [32]. In this paper, to develop an *n*-type SKD TE joint that is qualified for practical applications, we designed and fabricated *n*-type SKD joints with the structure of Ti/Mo/Yb_{0.3}Co₄Sb₁₂. In this structure, Ti is reserved as the bonding layer for its active bonding behavior with common electrode materials including Cu and Ni. Furthermore, Ti is also expected to buffer the interfacial thermal stress. To suppress the activity of Ti at a high temperature and also barrier the inter-diffusion between TE materials and the electrode, Mo is chosen as the barrier layer. Both Mo and Ti were deposited onto the Yb_{0.3}Co₄Sb₁₂ surface by magnetron sputtering to achieve flat interfaces. Because of the evident difference between the CTEs of Mo and Yb_{0.3}Co₄Sb₁₂, the thickness of the Mo layer was controlled to no more than 4.5 μm to decrease the thermal stress at high temperatures.

To reveal the interfacial diffusion kinetics of the Ti/Mo/Yb_{0.3}Co₄Sb₁₂ joints and predict their service life, the above *n*-type SKD TE joints were thermal shocked between 0 °C and 600 °C and isothermally aged between 550 °C and 650 °C. After each thermal shocking or isothermal aging step, the interfacial microstructures and the interfacial contact resistivity were both investigated. Based on

the measurement results, the diffusion kinetics were investigated and the service life was predicted at different temperatures.

2. Materials and Methods

The fabrication of the *n*-type $\text{Yb}_{0.3}\text{Co}_4\text{Sb}_{12}$ powder followed the same process described in reference [33]. To fabricate samples for the measurement of the coefficient of thermal expansion (CTE), $\text{Yb}_{0.3}\text{Co}_4\text{Sb}_{12}$ powder was loaded into a graphite die ($\Phi 30$ mm) and consolidated in a spark plasma sintering (SPS) system at 620 °C under a pressure of 60 MPa and held for 10 min. Ti powder (4 N, 45 μm) was loaded into a graphite die ($\Phi 30$ mm) and consolidated at 1100 °C under a pressure of 60 MPa and held for 20 min in the same SPS system. The final dimension of the samples for CTE measurement was $4 \times 4 \times 20$ mm^3 . To fabricate the Ti/Mo/ $\text{Yb}_{0.3}\text{Co}_4\text{Sb}_{12}$ joints, $\text{Yb}_{0.3}\text{Co}_4\text{Sb}_{12}$ powder was consolidated following the same sintering process as mentioned above. The surfaces of the resulting $\text{Yb}_{0.3}\text{Co}_4\text{Sb}_{12}$ bulks were polished and cleaned ultrasonically before they were dried and loaded into the chamber of a magnetron sputtering system. The chamber was evacuated to 3×10^{-3} Pa and heated to 150 °C before Ar was introduced. Mo was sputtered at 1.5 Pa under 1.5 kW for 50 min. Then, Ti was sputtered at 1.5 Pa under 3 kW for 120 min. The resulting samples were cut into joints with a final dimension of about $3 \times 3 \times 6$ mm^3 . The joints were then sealed in quartz ampoules under vacuum. In the thermal shocking test, the ampoules were moved from room temperature into a furnace at 600 °C and kept inside for 5 min. Then, they were taken out into a water tank at 0 °C for another 5 min. In the isothermal aging test, the ampoules were kept at 550 °C, 600 °C, and 650 °C for different time periods of time. The CTE were measured with a Linseis-L75VS dilatometer (Princeton Junction, Princeton, NJ, USA). The interfacial microstructure of the joints was investigated by a scanning electronic microscope (ZEISS, SUPRA-55-SAPPHIRE, Oberkochen, Germany), and the chemical composition of the interfacial diffusion layers was analyzed using an Energy Dispersive Spectrometer (OXFORD, X-MaxN, Oxfordshire, UK). The contact resistivity of the joints was measured on the homemade four-probe platform (Haida Tech, Beijing, China) mentioned in our previous paper [34]. All the data for the diffusion layer thickness and the contact resistivity presented in this paper are the root mean square of three parallel samples, and the error bars are the root mean square errors.

3. Results and Discussion

3.1. Thermal Shocking

Figure 1 shows the variation of the CTE with temperature for $\text{Yb}_{0.3}\text{Co}_4\text{Sb}_{12}$, Ti, Mo, and Cu & Ni, which are common electrode materials. Clearly the CTE mismatch between Ti and $\text{Yb}_{0.3}\text{Co}_4\text{Sb}_{12}$ (or Cu & Ni) is much less than that between Mo and $\text{Yb}_{0.3}\text{Co}_4\text{Sb}_{12}$ (or Cu & Ni). Based on Figure 2a,b, in the as prepared Ti/Mo/ $\text{Yb}_{0.3}\text{Co}_4\text{Sb}_{12}$ joints, the bonding between Ti, Mo and $\text{Yb}_{0.3}\text{Co}_4\text{Sb}_{12}$ is good with the thickness of the Mo layer being about 4.5 μm and the interfacial diffusion being neglectable at both the Ti/Mo and the Mo/ $\text{Yb}_{0.3}\text{Co}_4\text{Sb}_{12}$ interfaces. The Ti/Mo/ $\text{Yb}_{0.3}\text{Co}_4\text{Sb}_{12}$ joints then experienced thermal shocking for 10 cycles between 0 °C and 600 °C in vacuum. Figure 2c demonstrates that the bonding between Ti, Mo, and $\text{Yb}_{0.3}\text{Co}_4\text{Sb}_{12}$ remains good after 10 cycles of thermal shocking. Besides, the contact resistivity of the joints before and after thermal shocking was measured to be around 3.9 $\mu\Omega\cdot\text{cm}^2$ and 3.7 $\mu\Omega\cdot\text{cm}^2$, respectively. Based on the above results, it can be concluded that in spite of evident CTE mismatch between Mo and $\text{Yb}_{0.3}\text{Co}_4\text{Sb}_{12}$, the interfacial bonding of the Ti/Mo/ $\text{Yb}_{0.3}\text{Co}_4\text{Sb}_{12}$ joints is quite strong and can survive severe thermal shocking. For these Ti/Mo/ $\text{Yb}_{0.3}\text{Co}_4\text{Sb}_{12}$ joints, because the Mo layer thickness is very small, the interfacial thermal stress from CTE mismatch is controlled at a relatively low level. Moreover, the Ti layer also helps to balance the CTE mismatch between Mo and $\text{Yb}_{0.3}\text{Co}_4\text{Sb}_{12}$ and release the interfacial thermal stress.

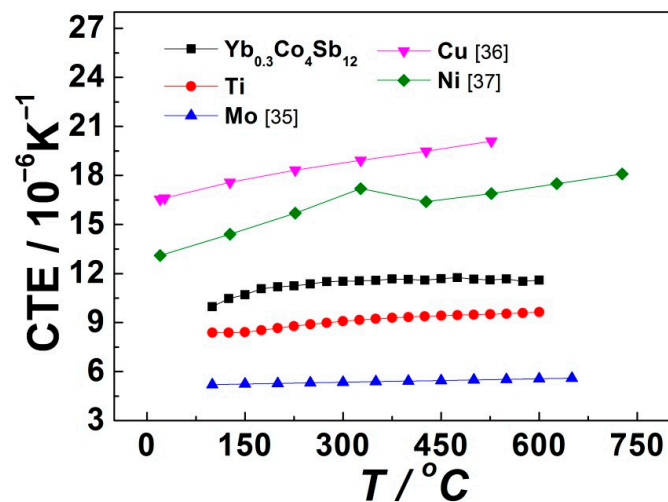


Figure 1. Variation of the CTE with temperature for $\text{Yb}_{0.3}\text{Co}_4\text{Sb}_{12}$, Ti, Mo, Cu, and Ni, Data for Mo, Cu, and Ni are from references [35–37] respectively.

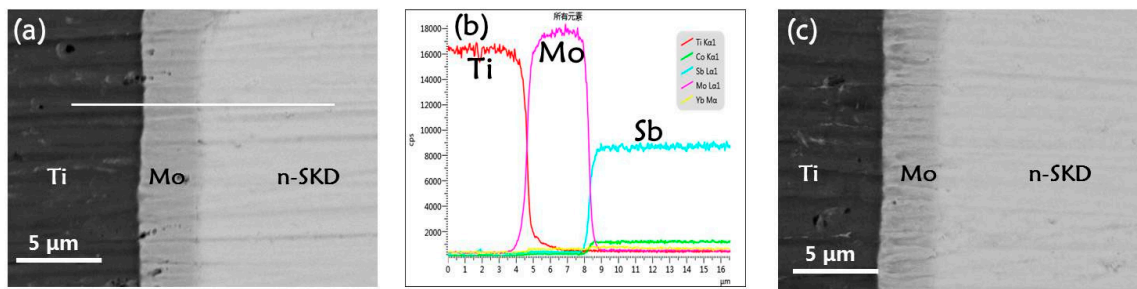


Figure 2. The interfacial microstructure of the Ti/Mo/ $\text{Yb}_{0.3}\text{Co}_4\text{Sb}_{12}$ joints (a), as prepared, a Back Scattering Electron (BSE) graph, (b), as prepared, a line scan, and (c), after 10 cycles of thermal shocking between 0 °C and 600 °C, a BSE graph.

3.2. Isothermal Aging

3.2.1. Pretreatment

The Ti/Mo/ $\text{Yb}_{0.3}\text{Co}_4\text{Sb}_{12}$ joints were then pretreated by isothermal aging at 550 °C. Figure 3a,b show the BSE graph with spot testing results and line scan results across the interfaces of the joints after 16 days aging, respectively. Figure 3c shows the distribution of the Ti content in the joint and it clearly reveals that some Ti atoms have penetrated across the Mo layer and reached the $\text{Yb}_{0.3}\text{Co}_4\text{Sb}_{12}$ matrix. All the measurement results confirm that the inter-diffusion at the Mo/ $\text{Yb}_{0.3}\text{Co}_4\text{Sb}_{12}$ interface is neglectable. However, Ti diffuses across the Ti/Mo interface and moves into the Mo layer, consequently forming a new Mo-Ti layer with a content gradient. In the Mo-Ti layer, the content of Ti decreases from about 10 at % Ti at the Ti/Mo-Ti interface to about 5 at % Ti at the Mo-Ti/ $\text{Yb}_{0.3}\text{Co}_4\text{Sb}_{12}$ interface. The contact resistivity of about $3.8 \mu\Omega\cdot\text{cm}^2$ for the pretreated joints is almost the same value as that of the as prepared ones, which indicates that the penetration of the Ti atoms into the Mo layer almost does not affect the apparent contact resistivity of the joints. Furthermore, if one prolongs the pretreatment time, the inter-diffusion between the Ti and $\text{Yb}_{0.3}\text{Co}_4\text{Sb}_{12}$ matrix will surely begin.

Based on the above results, to simplify the study on the interfacial stability, all the following Ti/Mo/ $\text{Yb}_{0.3}\text{Co}_4\text{Sb}_{12}$ joints were pretreated at 550 °C for 16 days before they were further isothermally aged. Correspondingly, the structure of the joints after the pretreatments is referred to as Ti/Mo-Ti/ $\text{Yb}_{0.3}\text{Co}_4\text{Sb}_{12}$ and the end of the pretreatment is set to be the beginning of the isothermal aging.

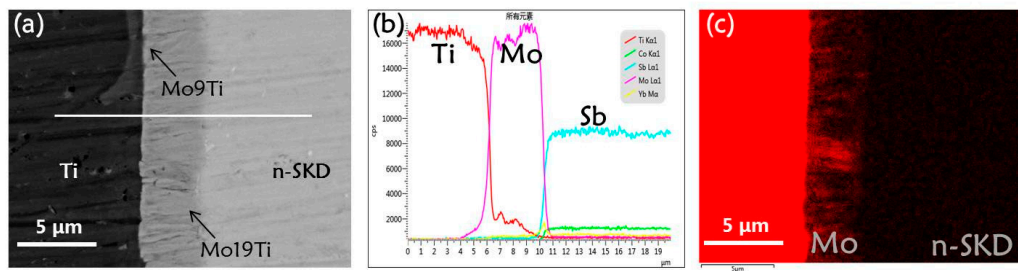


Figure 3. The interfacial microstructure of the Ti/Mo/Yb_{0.3}Co₄Sb₁₂ joints pretreated at 550 °C for 16 days. (a) the BSE graph and spot testing, (b) line scan results, (c) the distribution of Ti.

3.2.2. Diffusion Kinetics of the Interface

The pretreated joints were then isothermally aged at 550 °C and the inter-diffusion between Ti and Yb_{0.3}Co₄Sb₁₂ occurred at the Mo-Ti/Yb_{0.3}Co₄Sb₁₂ interface. The BSE graphs of the interfacial cross section for the joints after 20-day and 50-day aging are shown in Figure 4a,b. After being aged for 50 days, the diffusion layer is about 0.3 μm thick and consists of about 90 at % Ti and 10 at % Sb without any sign of Mo. The extremely slow growth-speed of the diffusion layer implies that the new Mo-Ti layer formed in the pretreatment effectively dampens the diffusion of Ti atoms before they reach the Yb_{0.3}Co₄Sb₁₂ matrix. Besides, Figure 4c,d show that there is no evident change in the distribution of Ti and Mo in the formed Mo-Ti layer, compared to the pretreated joints.

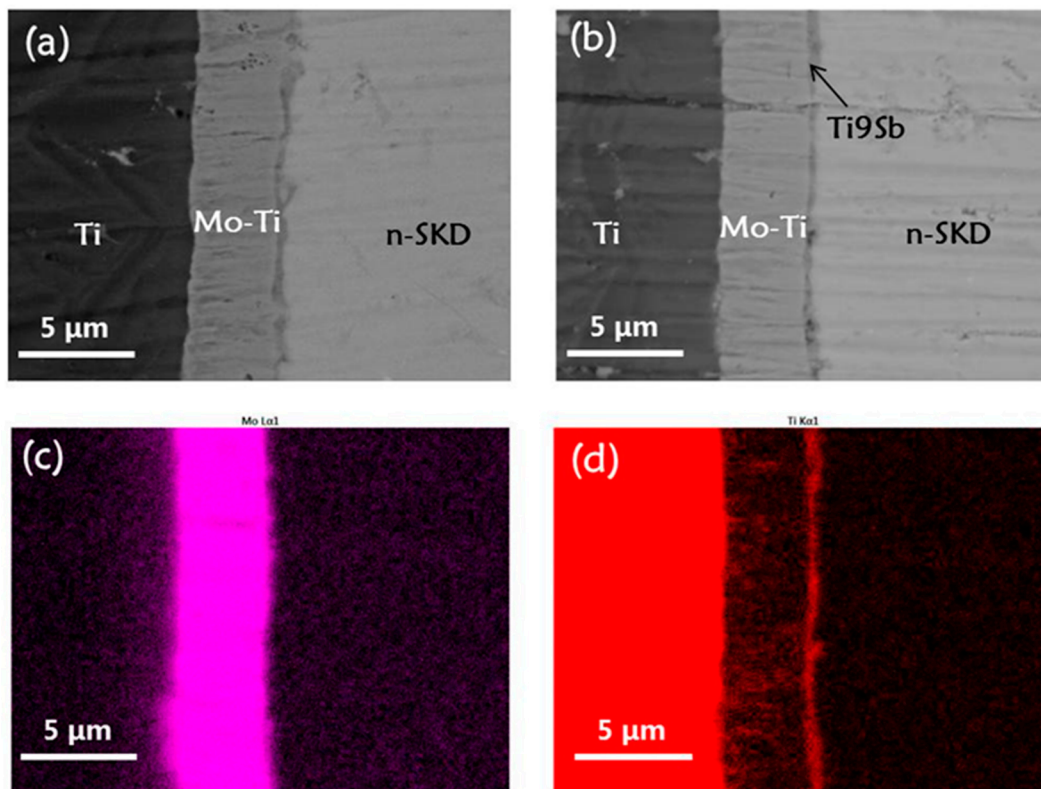


Figure 4. The interfacial evolution of the pretreated joints isothermally aged at 550 °C. (a) BSE graph, 20 days; (b) BSE graph, 50 days; (c) distribution of Mo, 50 days; (d) distribution of Ti, 50 days.

The pretreated joints were also isothermally aged at 600 °C and 650 °C. It was found that the growth rate of the diffusion layer between Ti and Yb_{0.3}Co₄Sb₁₂ increases with an increasing aging temperature. According to Figure 5, after being aged at 600 °C for 41 days, the diffusion layer at the

Mo-Ti/Yb_{0.3}Co₄Sb₁₂ interface reaches about 2 μm and consists of two sub-layers of Ti₃Sb and Ti₂Sb. Figure 6 shows that after being aged for nine days at 650 °C, the total thickness of the diffusion layer at the Mo-Ti/Yb_{0.3}Co₄Sb₁₂ interface grows to about 4.5 μm. Beside the sub-layers of Ti₃Sb and Ti₂Sb, there also appears a sign of TiCoSb in the front of the diffusion layer.

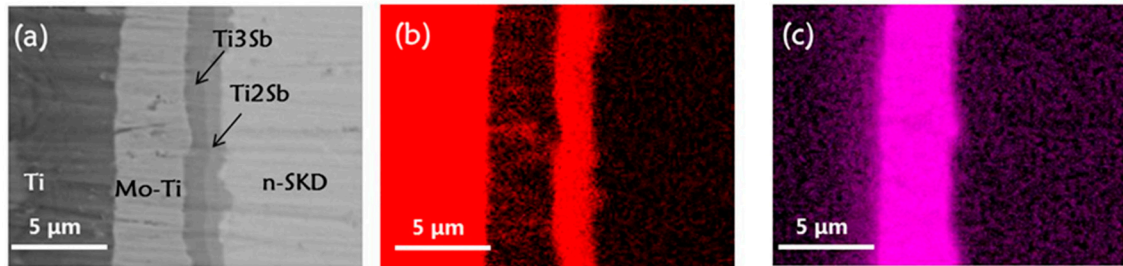


Figure 5. The interfacial microstructure of the pretreated joints isothermally aged at 600 °C for 41 days. (a) BSE graph and spot testing, (b) distribution of Ti, (c) distribution of Mo.

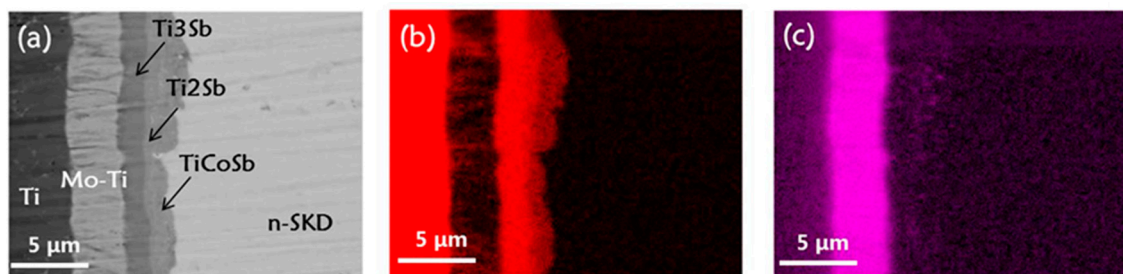


Figure 6. The interfacial microstructure of the pretreated joints isothermally aged at 650 °C for nine days. (a) BSE graph and spot testing, (b) distribution of Ti, (c) distribution of Mo.

To reveal the diffusion kinetics, we analyzed the relationship between the total diffusion layer thickness, aging time, and aging temperature. Figure 7a shows that at all the three aging temperatures, the total thickness of the diffusion layer is linear with the square root of the aging time, which indicates that the evolution of the Mo-Ti/Yb_{0.3}Co₄Sb₁₂ interface is a diffusion-controlling process between 550 °C and 650 °C. Therefore, the diffusion layer thickness can be expressed by the following parabolic equation [38,39]:

$$Y - Y_0 = (Dt)^{0.5} \quad (1)$$

where t is the aging time, and Y_0 and Y are the total diffusion layer thickness at the origin of aging and after being aged for a time period of t , respectively. D is the growth rate of the diffusion layer, which is a function of the aging temperature. By fitting the data of the diffusion layer thickness as a function of $t^{0.5}$, $D^{0.5}$, which is the slope of the fitting result, can be obtained.

To determine the activation energy for the interfacial diffusion, the Arrhenius relationship was used,

$$D = D_0 \exp\left(-\frac{Q}{RT}\right) \quad (2)$$

where D_0 is the growth constant, Q is the apparent activation energy for the growth of the total diffusion layer, T is the temperature in Kelvin, and R is the gas constant, 8.314 J/(mol·K). Equation (2) can be transformed into:

$$\ln D = -\frac{Q}{1000R} \cdot \frac{1000}{T} + D_0 \quad (3)$$

By plotting and fitting $\ln D$ against $1000/T$, Q can be obtained. Table 1 shows detailed D values and relations between the diffusion layer thickness and aging time. As is shown in Figure 7b, based on Table 1 and Equation (3), the activation energy Q for the growth of the diffusion layer at the

Mo-Ti/Yb_{0.3}Co₄Sb₁₂ interface is calculated to be about 447.5 kJ/mol at the temperature range of 550 °C to 650 °C. Combined with the above results, the variation of the diffusion layer thickness at the Mo-Ti/Yb_{0.3}Co₄Sb₁₂ interface can be predicted over the above temperature range.

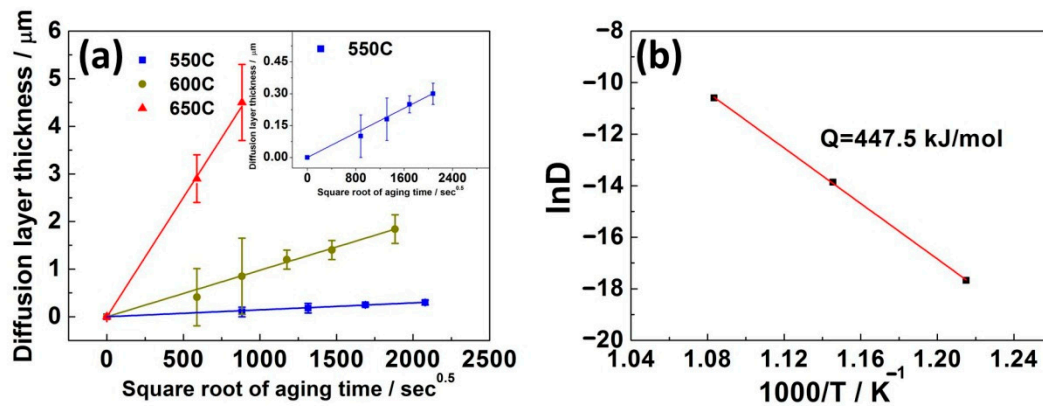


Figure 7. (a) Variation of the diffusion layer thickness of the pretreated joints with the square root of aging time between 550 °C and 650 °C. The inset is the enlargement of the result at 550 °C. (b) Variation of lnD with 1000/T between 550 °C and 650 °C.

Table 1. Fitting results of the growth rate and the relationship between diffusion layer thickness and aging time (s).

Temperature/°C	D/10 ⁻¹⁹ m ² /s	Y/μm
550	0.21	1.45 × 10 ⁻⁴ · t ^{0.5}
600	9.53	9.76 × 10 ⁻⁴ · t ^{0.5}
650	251	50.1 × 10 ⁻⁴ · t ^{0.5}

3.2.3. Stability of the Contact Resistivity and Service Life Prediction

To study the high temperature stability of the electrical properties of these joints, the contact resistivity of the joints was measured after each different thermal aging time. Figure 8 exhibits the variation of the interfacial contact resistivity of the joints with the square root of the aging time between 550 °C and 650 °C. At the aging temperature of 550 °C, the contact resistivity of the joint increases very slowly and reaches about 4.5 μΩ·cm² after being aged for 50 days. Increasing the aging temperature to 600 °C and 650 °C, the contact resistivity reaches 6.8 μΩ·cm² and 10 μΩ·cm² after 41 days and nine days, respectively. In contrast to the previous reports [26,29–31], the stability of the contact resistivity of the Ti/Mo/Yb_{0.3}Co₄Sb₁₂ joints is significantly improved.

The variation of the contact resistivity was then fitted with the square root of the aging time and a linear relationship between them was found (See Table 2). Based on Tables 1 and 2, it is clear that the increase in the contact resistivity of the Ti/Mo-Ti/Yb_{0.3}Co₄Sb₁₂ joints corresponds well to the increase in the thickness of the interfacial diffusion layer at the Mo-Ti/Yb_{0.3}Co₄Sb₁₂ interface. In another word, it is the growth of the interfacial diffusion layer at the Mo-Ti/Yb_{0.3}Co₄Sb₁₂ interface that dominates the stability of the interfacial contact resistivity of the Ti/Mo-Ti/Yb_{0.3}Co₄Sb₁₂ joints.

The performance of the TE joints, as well as that of the TEGs, is sensitive to the contact resistivity, and therefore, the contact resistivity is a valuable criteria for the service life prediction of the TE joints. We assume that a Ti/Mo/Yb_{0.3}Co₄Sb₁₂ joint fails when the interfacial contact resistivity reaches 10 μΩ·cm² or 20 μΩ·cm², which are low values and satisfy most practical applications, and the service life of the joint is then predicted in Table 2. At the service temperature of 550 °C, the pretreated Ti/Mo/Yb_{0.3}Co₄Sb₁₂ joints can endure about 21 years before the contact resistivity reaches 10 μΩ·cm². Even when increasing the service temperature to 600 °C, the joints can survive for 3.9 years before the contact resistivity reaches 20 μΩ·cm².

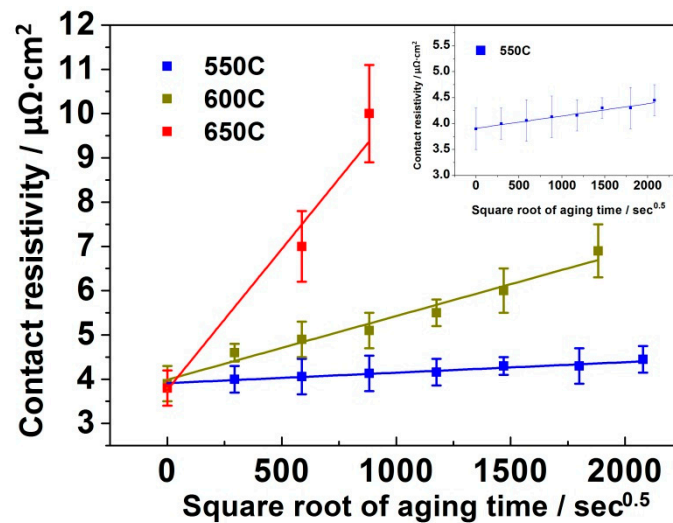


Figure 8. Variation of the interfacial contact resistivity of the joints with the square root of the aging time between 550 °C and 650 °C.

Table 2. Fitting results of the relationship between the contact resistivity and the aging time, and predicted service life (The prediction is based on the assumption that a joint fails when the contact resistivity reaches 10 $\mu\Omega\cdot\text{cm}^2$ (a) and 20 $\mu\Omega\cdot\text{cm}^2$ (b)).

Temperature/°C	Contact Resistivity/ $\mu\Omega\cdot\text{cm}^2$	Predicted Service life ^(a) /day	Predicted Service life ^(b) /day
550	$2.37 \times 10^{-4} \cdot t^{0.5} + 3.91$	7642	53,346
600	$14.1 \times 10^{-4} \cdot t^{0.5} + 3.99$	201	1431
650	$63.5 \times 10^{-4} \cdot t^{0.5} + 3.76$	11	75

4. Conclusions

In this paper, we successfully designed and fabricated *n*-type SKD thermoelectric joints with the sandwich structures of Ti/Mo/Yb_{0.3}Co₄Sb₁₂. With a controlled Mo layer thickness and the buffering of the Ti layer, the interfaces of the joints bond well and can survive severe thermal shocking. During isothermal aging at the temperature range of 550 °C to 650 °C, Ti penetrates across the Mo layer and diffuses into the Yb_{0.3}Co₄Sb₁₂ matrix. The interfacial evolution at the formed Mo-Ti/Yb_{0.3}Co₄Sb₁₂ interface is found to be a diffusion-controlling process. Diffusion kinetics between Ti and Yb_{0.3}Co₄Sb₁₂ at the Mo-Ti/Yb_{0.3}Co₄Sb₁₂ interface were investigated and the apparent activation energy for the growth of the diffusion layer was obtained. Meanwhile, it was also found that the inter-diffusion between Ti and Yb_{0.3}Co₄Sb₁₂ is the decisive factor in the rise of the contact resistivity. Because of the damping of the formed Mo-Ti layer, the diffusion of Ti towards the Yb_{0.3}Co₄Sb₁₂ is greatly decelerated and the inter-diffusion between the Ti and the Yb_{0.3}Co₄Sb₁₂ matrix is extremely slow. As a result, the Ti/Mo/Yb_{0.3}Co₄Sb₁₂ joints demonstrate the excellent stability of the contact resistivity. Based on the stability of the contact resistivity, service life prediction of the joints was made, and the result shows that the Ti/Mo/Yb_{0.3}Co₄Sb₁₂ joint is a qualified choice and a promising candidate for practical applications at 550 °C and 600 °C in vacuum, respectively.

Acknowledgments: The authors acknowledge the financial supports from the National Natural Science Foundation of China (Contract No. 51404236, 51572282 and 51372261).

Author Contributions: Ming Gu conceived, designed, and performed the experiments, analyzed the data and wrote the paper. Shengqiang Bai instructed the designing of the experiments, the analyses of the data, and the writing of the paper. Xugui Xia helped to perform the experiments and analyses of the data. Xiangyang Huang and Xiaoya Li supported the analyses of the data through valuable discussions. Xun Shi and Lidong Chen supported and provided guideline of the work.

Conflicts of Interest: The authors declare no conflict of interest.

References

1. Mohamed, S.E.G.; Saber, H.H. High efficiency segmented thermoelectric unicouple for operation between 973 and 300 K. *Energy Convers. Manag.* **2003**, *44*, 1069–1088.
2. Mohamed, S.E.G.; Saber, H.H. Thierry Caillat, Efficient segmented thermoelectric unicouples for space power applications. *Energy Convers. Manag.* **2004**, *44*, 1755–1772.
3. Salzgeber, K.; Prenninger, P.; Grytsiv, A.; Rogl, P.; Bauer, E. Skutterudites: Thermoelectric Materials for Automotive Applications? *J. Electron. Mater.* **2010**, *39*, 2074–2078. [[CrossRef](#)]
4. Kumar, S.; Heister, S.D.; Xu, X.; Salvador, J.R. Optimization of thermoelectric components for automobile waste heat recovery systems. *J. Electron. Mater.* **2015**, *44*, 3627–3636. [[CrossRef](#)]
5. Lu, Z.; Zhang, H.; Mao, C.; Li, C.M. Silk fabric-based wearable thermoelectric generator for energy harvesting from the human body. *Appl. Energy* **2016**, *164*, 57–63. [[CrossRef](#)]
6. Gelbstein, Y.; Tunbridge, J.; Dixon, R.; Reece, M.J.; Ning, H.P.; Gilchrist, R.; Summers, R.; Agote, I.; Lagos, M.A.; Simpson, K.; et al. Physical, mechanical and structural properties of highly efficient nanostructured *n*- and *p*- silicides for practical thermoelectric applications. *J. Electron. Mater.* **2014**, *43*, 1703–1711. [[CrossRef](#)]
7. Joshi, G.; Lee, H.; Lan, Y.; Wang, X.; Zhu, G.; Wang, D.; Gould, R.W.; Cuff, D.C.; Tang, M.Y.; Dresselhaus, M.S.; et al. Enhanced thermoelectric figure-of-merit in nanostructured p-type silicon germanium bulk alloys. *Nano Lett.* **2008**, *8*, 4670–4674. [[CrossRef](#)] [[PubMed](#)]
8. Wang, X.W.; Lee, H.; Lan, Y.C.; Zhu, G.H.; Joshi, G.; Wang, D.Z.; Yang, J.; Muto, A.J.; Tang, M.Y.; Klatsky, J.; et al. Enhanced thermoelectric figure of merit in nanostructured *n*-type silicon germanium bulk alloy. *Appl. Phys. Lett.* **2008**, *93*, 193121.
9. Yang, X.; Wu, J.; Ren, D.; Zhang, T.; Chen, L. Microstructure and Thermoelectric Properties of *p*-type $\text{Si}_{80}\text{Ge}_{20}\text{B}_{0.6}$ -SiC Nanocomposite. *J. Inorg. Mater.* **2016**, *31*, 997–1003.
10. Appel, O.; Schwall, M.; Kohne, M.; Balke, B.; Gelbstein, Y. Effects of microstructural evolution effects on the thermoelectric properties of spark plasma sintered $\text{Ti}_{0.3}\text{Zr}_{0.35}\text{Hf}_{0.35}\text{NiSn}$ half-Heusler compound. *J. Electron. Mater.* **2013**, *42*, 1340–1345. [[CrossRef](#)]
11. Appel, O.; Zilber, T.; Kalabukhov, S.; Beerli, O.; Gelbstein, Y. Morphological effects on the thermoelectric properties of $\text{Ti}_{0.3}\text{Zr}_{0.35}\text{Hf}_{0.35}\text{Ni}_{1+\delta}\text{Sn}$ alloys following phase separation. *J. Mater. Chem.* **2015**, *3*, 11653–11659.
12. Vizel, R.; Bargig, T.; Beerli, O.; Gelbstein, Y. Bonding of Bi_2Te_3 based thermoelectric legs to metallic contacts using $\text{Bi}_{0.82}\text{Sb}_{0.18}$ alloy. *J. Electron. Mater.* **2016**, *45*, 1296–1300. [[CrossRef](#)]
13. Lee, M.H.; Rhyee, J.; Kim, S.; Choa, Y. Thermoelectric properties of $\text{Bi}_{0.5}\text{Sb}_{1.5}\text{Te}_3/\text{Ag}_2\text{Te}$ bulk composites with size- and shape-controlled Ag_2Te nano-particles dispersion. *J. Alloys Compd.* **2016**, *657*, 639–645. [[CrossRef](#)]
14. Sumithra, S.; Takas, N.J.; Misra, D.K.; Nolting, W.M.; Poudeu, P.F.P.; Stokes, K.L. Enhancement in thermoelectric figure of merit in nanostructured Bi_2Te_3 with semimetal nanoinclusions. *Adv. Energy Mater.* **2011**, *1*, 1141–1147. [[CrossRef](#)]
15. Mei, D.; Li, Y.; Yao, Z.; Wang, H.; Zhu, T.; Chen, S. Enhanced thermoelectric performance of *n*-type PbTe bulk materials fabricated by semisolid powder processing. *J. Alloys Compd.* **2014**, *609*, 201–205. [[CrossRef](#)]
16. Li, J.Q.; Lu, Z.W.; Li, S.M.; Liu, F.S.; Ao, W.Q.; Li, Y. High thermoelectric properties of PbTe-Sm₂Se₃ composites. *Scripta Mater.* **2016**, *112*, 144–147. [[CrossRef](#)]
17. Gelbstein, Y. $\text{Pb}_{1-x}\text{Sn}_x\text{Te}$ Alloys—Application Considerations. *J. Electron. Mater.* **2011**, *40*, 533–536. [[CrossRef](#)]
18. Gelbstein, Y. Phase morphology effects on the thermoelectric properties of $\text{Pb}_{0.25}\text{Sn}_{0.25}\text{Ge}_{0.5}\text{Te}$. *Acta Mater.* **2013**, *61*, 1499–1507. [[CrossRef](#)]
19. Dado, B.; Gelbstein, Y.; Mogilansky, D.; Ezersky, V.; Dariel, M.P. Structural evolution following spinodal decomposition of the pseudo-ternary compound $(\text{Pb}_{0.3}\text{Sn}_{0.1}\text{Ge}_{0.6})\text{Te}$. *J. Electron. Mater.* **2010**, *39*, 2165–2171. [[CrossRef](#)]
20. Hazan, E.; Ben-Yehuda, O.; Madar, N.; Gelbstein, Y. Functional graded germanium-lead chalcogenides-based thermoelectric module for renewable energy applications. *Adv. Energy Mater.* **2015**, *5*. [[CrossRef](#)]
21. Chen, L.; Backhaus-Ricoult, M.; He, L.; Li, X.; Xia, X.; Zhao, D. Fabrication Method for Thermoelectric Device. U.S. Patent US8198116 B2, 12 June 2012.
22. Ting, W.; Bai, S.; Shi, X.; Chen, L. Enhanced Thermoelectric Properties of $\text{Ba}_x\text{Eu}_y\text{Co}_4\text{Sb}_{12}$ with Very High Filling Fraction. *J. Inorg. Mater.* **2013**, *28*, 224–228.

23. Muto, A.; Yang, J.; Poudel, B.; Ren, Z.; Chen, G. Skutterudite unicouple characterization for energy harvesting applications. *Adv. Energy Mater.* **2013**, *3*, 245–251. [[CrossRef](#)]
24. Alleno, E.; Lamquembe, N.; Cardoso-Gil, R.; Ikeda, M.; Widder, F.; Rouleau, O.; Godart, C.; Grinl, Y.; Paschen, S. A thermoelectric generator based on an *n*-type clathrate and a *p*-type skutterudite unicouple. *Phys. Status Solidi A* **2014**, *1*, 1293–1300. [[CrossRef](#)]
25. Salvador, J.R.; Cho, J.Y.; Ye, Z.; Moczygamba, J.E.; Thompson, A.J.; Sharp, J.W.; Koenig, J.; Maloney, R.; Thompson, T.; Sakamoto, J.; et al. Conversion efficiency of skutterudite-based thermoelectric modules. *Phys. Chem. Chem. Phys.* **2014**, *16*, 12510–12520. [[CrossRef](#)] [[PubMed](#)]
26. Tang, Y.; Bai, S.; Ren, D.; Liao, J.; Zhang, L.; Chen, L. Interface Structure and Electrical Property of Yb_{0.3}Co₄Sb₁₂/Mo-Cu Element Prepared by Welding Using Ag-Cu-Zn Solder. *J. Inorg. Mater.* **2015**, *30*, 256–260.
27. Fan, J.; Chen, L.; Bai, S.; Shi, X. Joining of Mo to CoSb₃ by spark plasma sintering by inserting a Ti interlayer. *Mater. Lett.* **2004**, *58*, 3876–3878. [[CrossRef](#)]
28. Zhao, D.; Li, X.; He, L.; Jiang, W.; Chen, L. Interfacial evolution behavior and reliability evaluation of CoSb₃/Ti/Mo-Cu thermoelectric joints during accelerated thermal aging. *J. Alloys Compd.* **2009**, *477*, 425–431. [[CrossRef](#)]
29. Zhao, D.; Li, X.; He, L.; Jiang, W.; Chen, L. High temperature reliability evaluation of CoSb₃/electrode thermoelectric joints. *Intermetallics* **2009**, *17*, 136–141. [[CrossRef](#)]
30. Gu, M.; Xia, X.; Li, X.; Huang, X.; Chen, L. Microstructural evolution of the interfacial layer in the Ti-Al/Yb_{0.6}Co₄Sb₁₂ thermoelectric joints at high temperature. *J. Alloys Compd.* **2014**, *610*, 665–670. [[CrossRef](#)]
31. Fan, X.C.; Gu, M.; Shi, X.; Chen, L.D.; Bai, S.Q.; Nunna, R. Fabrication and reliability evaluation of Yb_{0.3}Co₄Sb₁₂/Mo-Ti/Mo-Cu/Ni thermoelectric joints. *Ceram. Int.* **2015**, *41*, 7590–7595. [[CrossRef](#)]
32. Bae, K.H.; Choi, S.; Kim, K.; Choi, H.; Seo, W.; Kim, I.; Lee, S.; Hwang, H.J. Power-Generation Characteristics After Vibration and Thermal Stresses of Thermoelectric Unicouples with CoSb₃/Ti/Mo(Cu) Interfaces. *J. Electron. Mater.* **2015**, *44*, 2124–2131. [[CrossRef](#)]
33. Zhao, X.Y.; Shi, X.; Chen, L.D.; Zhang, W.Q.; Zhang, W.B.; Pei, Y.Z. Synthesis and thermoelectric properties of Sr-filled skutterudite Sr_yCo₄Sb₁₂. *J. Appl. Phys.* **2006**, *99*, 053711. [[CrossRef](#)]
34. Gu, M.; Xia, X.; Huang, X.; Bai, S.; Li, X.; Chen, L. Study on the interfacial stability of *p*-type Ti/Ce_yFe_xCo_{4-x}Sb₁₂ thermoelectric joints at high temperature. *J. Alloys Compd.* **2016**, *671*, 238–244. [[CrossRef](#)]
35. PLANSEE. Available online: <https://www.plansee.com/en/materials/molybdenum.html> (accessed on 22 August 2017).
36. Hahn, T.A. Thermal Expansion of Copper from 20 to 800 K—Standard Reference Material 736. *J. Appl. Phys.* **1970**, *41*, 5096–5101. [[CrossRef](#)]
37. Abdullaev, R.N.; Kozlovskii, Y.M.; Khairulin, R.A.; Stankus, S.V. Density and Thermal Expansion of High Purity Nickel over the Temperature Range from 150 K to 2030 K. *Int J Thermophys.* **2015**, *36*, 603–619. [[CrossRef](#)]
38. Yu, D.Q.; Wang, L. The growth and roughness evolution of intermetallic compounds of Sn–Ag–Cu/Cu interface during soldering reaction. *J. Alloys Compd.* **2008**, *458*, 542–547. [[CrossRef](#)]
39. Sun, P.; Andersson, C.; Wei, X.; Cheng, Z.; Shangguan, D.; Liu, J. Study of interfacial reactions in Sn–3.5Ag–3.0Bi and Sn–8.0Zn–3.0Bi sandwich structure solder joint with Ni(P)/Cu metallization on Cu substrate. *J. Alloys Compd.* **2007**, *437*, 169–179. [[CrossRef](#)]

